Pion and kaon fragmentation functions at next-to-next-to-leading order

Rabah Abdul Khalek [a], Valerio Bertone [b], Alice Khoudli [b], Emanuele R. Nocera [c,*]

[a] *Jefferson Lab, Newport News, VA 23606, USA*
[b] *IRFU, CEA, Université Paris-Saclay, F-91191 Gif-sur-Yvette, France*
[c] *The Higgs Centre for Theoretical Physics, University of Edinburgh, JCMB, KB, Mayfield Rd, Edinburgh EH9 3JZ, Scotland, United Kingdom*

A R T I C L E   I N F O

A B S T R A C T

We present a new determination of unpolarised charged pion and kaon fragmentation functions from a set of single-inclusive electron-positron annihilation and lepton-nucleon semi-inclusive deep-inelastic scattering data. The determination includes next-to-next-to-leading order QCD corrections to both processes, and is carried out in a framework that combines a neural-network parametrisation of fragmentation functions with a Monte Carlo representation of their uncertainties. We discuss the quality of the determination, in particular its dependence on higher order corrections.

1. Introduction

In a recent paper [1], we presented a determination of the fragmentation functions (FFs) [2] of charged pions from an analysis of hadron-production measurements in single-inclusive electron-positron annihilation (SIA) and semi-inclusive deep-inelastic scattering (SIDIS). The analysis, accurate to next-to-leading order (NLO) in perturbative quantum chromodynamics (QCD), utilised a framework that combines a neural network parametrisation of FFs (optimised through knowledge of the analytical derivative of neural networks with respect to their parameters) with a Monte Carlo representation of FF uncertainties. This approach — which has been extensively used by the NNPDF Collaboration to determine the parton distribution functions (PDFs) of the proton [3–6] and of nuclei [7–9] — allowed us to reduce model bias in FF parametrisation as much as possible, and to faithfully propagate experimental and PDF uncertainties into FFs. These features are essential to achieve the methodological accuracy of FFs that are utilised to analyse, *e.g.*, high-precision hadron production measurements at the Large Hadron Collider (LHC) and, in the future, at the Electron Ion Collider (EIC) [10].

Methodological accuracy is however only one component of the overall accuracy of the FF determination. Other important components are the accuracy of the experimental and theoretical inputs that also enter the FF determination. Regarding experimental accuracy, interplay between SIA and SIDIS measurements was studied

at length in Ref. [1], and the latter were found to be essential to constrain FFs for individual quark flavours. The two classes of measurements are indeed sensitive to different quark FF combinations due to the way in which the corresponding observables factorise [11]. Regarding theoretical accuracy, derivation of approximate next-to-next-to-leading order (NNLO) corrections to SIDIS, obtained from expansion of the resummed expressions, have been completed a few months ago [12].[1] Given the long-standing availability of NNLO corrections to SIA [14–16], and to time-like evolution [17–19], it is therefore natural to extend the framework developed in Ref. [1] to NNLO. This is the goal of this paper, in which we complement the original pion MAPFF1.o FF sets [1] with their NNLO counterparts.

We also produce analogous kaon FF sets, both at NLO and NNLO. Together with pions, kaons represent the most copiously produced hadrons in high-energy particle collisions. An accurate knowledge of kaon FFs is of crucial importance to use SIDIS measurements (including when the initial-state proton is longitudinally polarised) to constrain the (polarised) strange quark and anti-quark PDFs.

The MAPFF1.o pion and kaon FF sets presented in this paper extend the available NNLO analyses that are based solely on SIA measurements [20,21], as well as the very recent (and to date only) NNLO global analysis of pion FFs based on SIA and SIDIS measurements [22]. As for the previous determination [1], the NLO and NNLO MAPFF1.o pion and kaon FF sets are publicly delivered through the LHAPDF library [23]. The software developed to

---

[1] Approximate N[3]LO corrections have also been presented in Ref. [13].

produce them is also made open source [24]. In Sect. 2 we summarise the experimental, theoretical and methodological input to our analysis; in Sect. 3 we discuss the main results; and in Sect. 4 we present a summary and an outlook.

2. Experimental, theoretical, and methodological input

The SIA and SIDIS experimental measurements that are used as input to this analysis closely follow those of our previous work. For pions, we use exactly the same measurements as in Ref. [1], albeit with a different treatment of experimental uncertainties for the COMPASS data [25], see below. For kaons, we use SIA measurements performed at CERN (ALEPH [26], DELPHI [27] and OPAL [28]), DESY (TASSO [29–31]), KEK (BELLE [32] and TOPAZ [33]) and SLAC (BABAR [34], TPC [35] and SLD [36]); we also use SIDIS measurements performed at CERN by COMPASS [37] and at DESY by HERMES [38].

In the case of SIA, the data corresponds to the sum of the cross section for the production of positively and negatively charged kaons, differential with respect to either the longitudinal momentum fraction z of the outgoing kaon carried by the fragmenting parton or the momentum of the measured kaon (see Sect. 2.2 in Ref. [21] for details). For BELLE, we use the measurement corresponding to an integrated luminosity $\mathcal{L} = 68$ fb^{-1} [32]. A more recent measurement, based on a larger luminosity $\mathcal{L} = 558$ fb^{-1}, exists [39]. However we do not consider it because of a poor control of the degree of correlation of systematic uncertainties, which typically exceed in magnitude uncorrelated statistical uncertainties (see Ref. [1]). For BABAR we use the *conventional* data set, as done in other analyses, see *e.g.* Refs. [21,40,41]. This is in contrast to the pion measurement, for which we use the *prompt* data set. The difference between the prompt and conventional data sets is that only primary hadrons or decay products from particles with lifetime τ shorter than about 10^{-11} s are retained in the former. While prompt and conventional cross sections differ by about 5–15% for pions, they are almost identical for kaons. As shown in previous analyses of pion FFs [21,42,43], the inclusion of the conventional pion data set leads to a significant deterioration of the statistical quality of the fit. For this reason we do not consider the BABAR conventional pion data set at all. For DELPHI and SLD, in addition to the inclusive measurements, we also consider flavour-tagged measurements, whereby the production of the observed kaon has been reconstructed from hadronisation of all light quarks or of a b quark.

In the case of SIDIS, the data corresponds to the hadron multiplicity, *i.e.* the SIDIS cross section normalised to the corresponding inclusive DIS cross section (see Sect. 3 in Ref. [1] for details). For HERMES, similarly to what we did in the case of pions, we consider the projection of the fully differential measurement as a function of the transferred energy Q^2 and of z in individual bins of the momentum fraction x carried by the incoming parton. We discard the bins with $z < 0.2$, which are used to control the model dependence of the smearing-unfolding procedure, and with $z > 0.8$, which lie in the region where the fractional contribution from exclusive processes is sizeable.

The kinematic coverage of the pion and kaon data is similar, see Sect. 2 of Ref. [1] for a detailed discussion. Kinematic cuts, to select only data points for which perturbative fixed-order predictions are reliable, are as in Ref. [1] for pions. Specifically, for SIA we retain only the data points that fall in the interval $[z_{\min}, z_{\max}]$, with $z_{\min} = 0.02$ for experiments at a centre-of-mass energy equal to M_Z and $z_{\min} = 0.075$ for all other experiments, and $z_{\max} = 0.9$ for all experiments. For SIDIS, we retain only the data points satisfying $Q > Q_{\text{cut}}$, with $Q_{\text{cut}} = 2$ GeV. In the case of kaons, we adopt exactly the same kinematic cuts as in the case of pions, with the exception of the value of $z_{\min}$ used for the BELLE and BABAR ex-

periments, which is set to 0.2. The reason being that the onset of small-z corrections at the centre-of-mass energy of B factories occurs for kaons at a higher value of z than it does for pions. We use the same set of cuts in the NLO and NNLO fits. In principle, different cuts could be defined depending on the perturbative order to maximise the amount of experimental information included in the fit. However, we prefer to be conservative, and use the same cuts determined in Ref. [1], where in particular a scan of the fit quality upon variation of Q_{cut} was performed. A similar study will be discussed further below, after which we will show that slightly less restrictive SIDIS cuts could be used without significantly spoiling the fit quality. However, these may alter the FF accuracy or precision, as we will also discuss.

Information on correlations of experimental uncertainties is taken into account whenever available, as detailed in Sect. 2 of Ref. [1]. In contrast to Ref. [1], however, we no longer consider the systematic uncertainty for the COMPASS measurements [25,37] to be 100% correlated across bins. We instead implement the recommendation to split the systematic uncertainty into two components, and take only the largest component (which amounts to 80% of the total systematic uncertainty) to be 100% correlated across bins. The remaining component is treated as fully uncorrelated, and is added in quadrature to the statistical uncertainty. This treatment is applied equally to pion and kaon measurements. In this respect, the NLO fit of pion FFs that we will present below differs from that of Ref. [1]. Further below we will also discuss how the fit quality and FFs are affected by variations in the treatment of experimental correlations in the COMPASS measurements.

The theoretical setup of our analysis closely follows that discussed in Sect. 3 of Ref. [1]. New to this determination is the inclusion of NNLO corrections to time-like DGLAP evolution equations and to SIA and SIDIS coefficient functions. Corrections to evolution equations and to SIA build upon various implementations and benchmarks carried out in previous work [21,44–46]. Corrections to SIDIS are instead taken from Ref. [12]. These corrections were derived using the threshold-resummation formalism. They are therefore approximate in that they only include the dominant contributions associated with the emission of soft gluons. Nevertheless, they are sufficiently accurate for our purpose: in Ref. [12] it was shown that the approximate and exact NLO results, which are both known, differ only by a tiny amount in the kinematic region relevant to the SIDIS data considered in this work (see Fig. 1 in Ref. [12]). The size of this difference is always largely smaller than the size of experimental uncertainties. It is reasonable to argue that the approximate NNLO result would not differ from the exact NNLO result, if known, by a larger amount. The unquantified uncertainty due to utilising the approximate, in lieu of the exact, result is therefore practically negligible. Furthermore, the inclusion of the dominant NNLO terms is expected to reduce the dependence of the cross section on the renormalisation and factorisation scales. This is what happens, as also shown in Ref. [12], see in particular Fig. 3 there. Finally, excellent perturbative stability of the SIDIS cross section was found very recently by extending the derivation in Ref. [12] to N^{3}LO [13].

As in Ref. [1], we use the NNPDF3.1 [5] PDF sets as input to the computation of SIDIS cross sections, specifically those obtained assuming that charm is perturbatively generated. The perturbative order of the PDF set is taken consistently with the perturbative order of the FF analysis. We have explicitly verified, *e.g.* by using the more recent NNPDF4.0 parton sets [6], that the dependence of our results on the choice of the PDFs is very weak, due to cancellations that occur in the multiplicity ratio, see also Ref. [1]. Because no heavy-quark mass corrections have been determined for SIDIS, our analysis is carried out in the zero-mass variable-flavour-number scheme. In this scheme all active partons are treated as massless, but a partial heavy-quark mass dependence is introduced

by requiring that sub-schemes with different numbers of active flavours match at the heavy-quark thresholds. The values of the charm- and bottom-quark thresholds are set to $m_c = 1.51$ GeV and $m_b = 4.92$ GeV, respectively, consistently with the NNPDF3.1 input PDF sets. Heavy-quark FFs are not set to zero below their respective thresholds, but are mathched[2] and kept constant, *i.e.* they do not evolve. Their contribution is suppressed by PDFs in SIDIS (see Sect. 3 in Ref. [1] for details). We finally note that isoscalarity of the SIDIS targets is taken into account by assuming exact SU(2) symmetry between protons and neutrons; no nuclear corrections are taken into account, as are no target or hadron mass corrections.

The statistical framework used in this analysis to infer FFs from experimental data is also the same as in Ref. [1]. Ingredients of the framework are the representation of experimental uncertainties into FFs by means of Monte Carlo sampling, and the parametrisation of FFs by means of neural networks. In the first respect, all of our FF sets are made of $N_{rep} = 200$ Monte Carlo replicas. In the case of SIDIS, a different PDF replica is chosen at random from the NNPDF3.1 parton set for each fitted FF replica. This ensures the propagation of PDF uncertainties into FFs. In the second respect, we consider, separately for pions and kaons, a single one-layered feed-forward neural network with one input node corresponding to the momentum fraction z, 20 intermediate nodes with a sigmoid activation function, and 7 output nodes with a linear activation function. This architecture amounts to a total of 187 parameters.

The output nodes correspond to the independent FFs of the positively charged hadrons that we fit. In the case of pions, these are given by Eq. (10) in Ref. [1]. In the case of kaons, these are obtained from those for pions by exchanging d and s quarks, that is:

$$\{D_u^{K^+}, \quad D_{\bar{s}}^{K^+}, \quad D_s^{K^+} = D_{\bar{u}}^{K^+}, \quad D_d^{K^+} = D_{\bar{d}}^{K^+},$$
$$D_c^{K^+} = D_{\bar{c}}^{K^+}, \quad D_b^{K^+} = D_{\bar{b}}^{K^+}, \quad D_g^{K^+}\}; \tag{1}$$

FFs for negatively charged hadrons are obtained from the positively charged ones by charge conjugation. The output nodes are squared to avoid large, unphysically negative FFs. The parametrisation is introduced at the initial scale $\mu_0 = 5$ GeV, as in our previous analysis [1]. Because this value is above the bottom quark threshold, we can parametrise the charm- and bottom-quark FFs, which receive large non-perturbative contributions, on the same footing as light quark FFs; FFs are then evolved to the scale of the SIDIS data (which can be lower than Q_0) in our fit. Our parametrisation does not include any power-like function to control the low- and high-z behaviours of FFs; however we require them to vanish at $z = 1$ by subtraction of the neural network itself, see also Ref. [21].

Optimisation of the neural network parameters is achieved by minimisation of the χ^2, see *e.g.* Eq. (21) in Ref. [1] for the exact definition used. Cross-validation is used to avoid overfitting, with a 50% training fraction for all of the data sets that contain more than 10 data points, otherwise the training fraction is 100%. Minimisation is realised with the Levenberg-Marquardt algorithm as implemented in the CERES SOLVER package [48]; analytical derivatives with respect to the parameters of the neural network are provided by the NNAD library [49].

3. Results and discussion

In Table 1 we report the number of data points, N_{dat}, and the value of the χ^2 per data point, χ^2/N_{dat}, for each data set included

in our pion and kaon fits at NLO and NNLO. Values corresponding to the SIA, SIDIS, and global data sets are also displayed. Inspection of Table 1 allows us to draw two observations.

First, we notice that the fit quality, as measured by the χ^2 per data point, reveals a generally good description of the entire data set, for both pions and kaons, and separately for SIA and SIDIS measurements. Anomalously small values of the χ^2 per data point are found for some data sets, that have low statistical significance because of either their limited number of data points (TASSO and HERMES) or their large uncorrelated uncertainties (BELLE), see Refs. [1,21]. The fit quality of the NLO pion fit is better than that found in Ref. [1]. The two fits, albeit based on the same data set and methodology, differ for the treatment of correlations in the COMPASS measurement. This is the reason for the reduction of the total χ^2 per data point from 0.90 in Ref. [1] to 0.68, as we will further discuss below.

Second, we notice that the dependence of the fit quality on the perturbative accuracy of the fit is opposite for pion and kaon FFs. When moving from NLO to NNLO, the total χ^2 per data point deteriorates from 0.68 to 0.76 in the former case, while it improves from 0.62 to 0.55 in the latter case. This behaviour is somewhat surprising given that NNLO corrections are independent from the hadron species. Also, the deterioration equally affects SIA and SIDIS data for pions, as does the improvement for kaons. The reasons for this behaviour, which differs from what was observed in a similar NNLO analysis [22], are only partly understood, as we will discuss below.

Figs. 1 and 2 display, for positively charged pions and kaons respectively, a comparison of the FFs (times the longitudinal momentum fraction z) obtained from our NLO and NNLO fits. For pions, we show $D_u^{\pi^+}$, $D_d^{\pi^+}$, $D_{\bar{d}}^{\pi^+}$, $D_{s^+}^{\pi^+}$, $D_{b^+}^{\pi^+}$ and $D_g^{\pi^+}$; for kaons, we show $D_u^{K^+}$, $D_s^{K^+}$, $D_{\bar{s}}^{K^+}$, $D_{d^+}^{K^+}$, $D_{b^+}^{K^+}$ and $D_g^{K^+}$. In both cases, FFs are displayed at the parametrisation scale $\mu = 5$ GeV, their expectation values and uncertainty bands correspond to the mean and standard deviation computed over the ensemble of FF replicas, and the lower insets display the FFs normalised to the NLO FFs.

Inspection of Figs. 1 and 2 reveals that inclusion of NNLO corrections results in a suppression of quark FFs, and in an enhancement of the gluon FF in the large-z region, $z \gtrsim 0.5$. This behaviour is expected: quark FFs ought to be suppressed to counteract the enhancement of theoretical predictions for SIA and SIDIS cross sections induced by NNLO corrections [12,50]. At the same time, the gluon FF is enhanced to accommodate stronger evolution effects. The size of the suppression depends on the quark flavour and on the hadron species: the instances in which this is more marked are for $D_u^{\pi^+}$, $D_d^{\pi^+}$, $D_{b^+}^{\pi^+}$, $D_u^{K^+}$, and $D_{b^+}^{K^+}$. In these cases, the suppression can be as large as 10-20%. By comparison, the quark FF uncertainty is only about a few percent. The enhancement of the gluon FF can be as large as 60%. Because the uncertainties on the gluon FF are significantly larger than for quark FFs, the enhancement is just such that the outer edges of the NLO and NNLO uncertainty bands touch each other: this corresponds to a $\sqrt{2}$ difference of a standard deviation. Be that as it may, in all of these cases the impact of NNLO corrections on FFs is statistically significant.

While the qualitative effect of NNLO corrections on the FFs displayed in Figs. 1-2 is expected, their quantitative effect on the pion FF fit is more difficult to interpret. In particular, it is surprising that the inclusion of NNLO corrections does not improve the fit quality, as already observed above. In an attempt to investigate the reason(s) for this behaviour, we have carried out a set of additional studies, which also served the purpose to test the stability of our results.

The first of such studies consists in varying the kinematic cut on the virtuality Q, Q_{cut}, in the analysis of SIDIS data. The study is similar to the one carried out in Sect. 5.3.3 of Ref. [1]: we have

---

Table 1

The number of data points, N_{dat}, and the χ^2 per data point, χ^2/N_{dat}, for each hadronic species and perturbative order considered in the fits of this analysis.

Experiment	Ref.	$h = \pi$			$h = K$		
		N_{dat}	χ^2/N_{dat} NLO	χ^2/N_{dat} NNLO	N_{dat}	χ^2/N_{dat} NLO	χ^2/N_{dat} NNLO
BELLE $h^{\pm}$	[32]	70	0.14	0.13	70	0.39	0.41
BABAR $h^{\pm}$	[34]	39	0.91	0.76	28	0.36	0.25
TASSO 12 GeV $h^{\pm}$	[29]	4	0.90	0.92	3	0.85	0.87
TASSO 14 GeV $h^{\pm}$	[30]	9	1.33	1.35	9	1.24	1.22
TASSO 22 GeV $h^{\pm}$	[30]	8	1.65	1.81	6	0.89	0.90
TPC $h^{\pm}$	[35]	13	0.23	0.25	13	0.38	0.40
TASSO 30 GeV $h^{\pm}$	[29]	2	0.30	0.34	–	–	–
TASSO 34 GeV $h^{\pm}$	[31]	9	1.08	1.48	5	0.07	0.06
TASSO 44 GeV $h^{\pm}$	[31]	6	1.13	1.37	–	–	–
TOPAZ $h^{\pm}$	[33]	5	0.24	0.37	3	0.10	0.11
ALEPH $h^{\pm}$	[26]	23	1.24	1.46	18	0.49	0.48
DELPHI (inclusive) $h^{\pm}$	[27]	21	1.31	1.25	23	0.97	0.99
DELPHI (*uds* tagged) $h^{\pm}$	[27]	21	2.68	2.89	23	0.44	0.38
DELPHI (*b* tagged) $h^{\pm}$	[27]	21	1.58	1.73	23	0.42	0.45
OPAL $h^{\pm}$	[28]	24	1.63	1.79	10	0.39	0.36
SLD (inclusive) $h^{\pm}$	[36]	34	1.05	1.13	35	0.83	0.67
SLD (*uds* tagged) $h^{\pm}$	[36]	34	1.59	2.16	35	1.37	1.52
SLD (*b* tagged) $h^{\pm}$	[36]	34	0.55	0.68	35	0.75	0.77
Total SIA		377	1.03	1.15	339	0.58	0.57
HERMES h^- d	[38]	2	0.41	0.32	2	0.18	0.13
HERMES h^+ p	[38]	2	0.01	0.02	2	0.05	0.04
HERMES h^- d	[38]	2	0.17	0.11	2	0.58	0.48
HERMES h^+ p	[38]	2	0.35	0.32	2	0.56	0.43
COMPASS h^-	[25,37]	157	0.48	0.55	156	0.74	0.59
COMPASS h^+	[25,37]	157	0.62	0.72	156	0.76	0.67
Total SIDIS		322	0.47	0.52	320	0.64	0.54
Global data set		**699**	**0.68**	**0.76**	**659**	**0.62**	**0.55**

repeated our NLO and NNLO fits, for both pions and kaons, varying the value of Q_{cut} in the range [1.00, 2.00] GeV in steps of 0.25 GeV. The value of the χ^2 per data point corresponding to the global data set for each of these fits is displayed in Fig. 3 for pions (left) and for kaons (right). The number of data points included in each fit is also indicated.

As one can see from Fig. 3, the value of the χ^2 per data point increases as the value of Q_{cut} is lowered, irrespective of the hadron species. Interestingly, for both pions and kaons, the rise is steeper at NNLO than at NLO; that is, the fit quality of the NNLO fit deteriorates much faster than that of the NLO fit as the value of Q_{cut} is decreased. While for pions, as already noted, the global χ^2 per data point is always larger at NNLO than at NLO, for kaons the rise is such that the quality of the NNLO fit becomes worse than that of the NLO fit if $Q_{cut} = 1$ GeV.

We have nevertheless verified that, in our framework, the fit quality of the pion FFs at NNLO is always better than its NLO counterpart if SIA or SIDIS data sets are fitted separately. This at least confirms that the expected perturbative convergence is recovered for each individual process. These fits have however exposed how relevant the interplay between SIA and SIDIS measurements is. On the one hand, the pion FFs determined by fitting only SIA data cannot be used to predict SIDIS data, because FFs for different quark flavours cannot be disentangled, see *e.g.* Sect. 3 in Ref. [21] and Sect. 3 in Ref. [1]. On the other hand, the pion FFs determined by fitting only SIDIS data do not provide a good description of SIA data, because the two classes of measurements probe somewhat disconnected kinematic regions, see *e.g.* Fig. 1 in Ref. [1]. In particular, SIDIS measurements probe FFs at rather low energies (a few GeV); they should therefore be evolved at higher energies (up to the Z-boson mass) with large extrapolation uncertainties. The reason why the quality of the pion FF NNLO fit becomes consistently worse than its NLO counterpart when SIA and SIDIS measurements are fitted together, be it the inconsistency of specific

data sets and/or the increased relevance of other theoretical corrections (such as power-suppressed corrections), is left to future study.

The deterioration of the quality of the pion FF fit upon reduction of the value of Q_{cut} has also partly been observed in Ref. [22]. There, however, the NNLO fit became worse than its NLO counterpart only for values of the cut on the virtuality $Q_{cut} \lesssim \sqrt{2.00}$ GeV. This is different from what we observe. Even if the analysis in Ref. [22] and ours are based on a similar data set, they however differ for the FF parametrisation and optimisation methodology. Understanding the origin of the discrepancy between the two sets of results would require a careful benchmark which goes beyond the scope of this paper.

However, the results in Ref. [22] and ours question whether, at such small values of Q, the leading-power factorisation framework used to describe SIDIS measurements is reliable. Poorly known power corrections, including interplay between initial- and final-state hadron mass effects [51,52], may become dominant, or the fragmentation regime may not even hold [53–55]. For all of these reasons, while the fit quality — as quantified by the value of the χ^2 per data point — may remain acceptable for values of Q_{cut} smaller than the one chosen as default in our fits ($Q_{cut} = 2$ GeV), we consider that the latter remains conservative against these effects. We have explicitly checked that the lower the value of Q_{cut}, the larger the distortion of the FFs (up to a couple of standard deviations at intermediate values of z for quark FFs), for either pions or kaons and irrespective of the perturbative order, in comparison to those displayed in Figs. 1 and 2.

The second study consists in investigating the role of the correlation model adopted to analyse the COMPASS SIDIS data. As already mentioned, in contrast to our previous analysis [1], we no longer assume the entirety of systematic uncertainties to be 100% correlated, but only a fraction of them equal to 80%. The remaining fraction of each systematic uncertainty is treated as fully uncor-
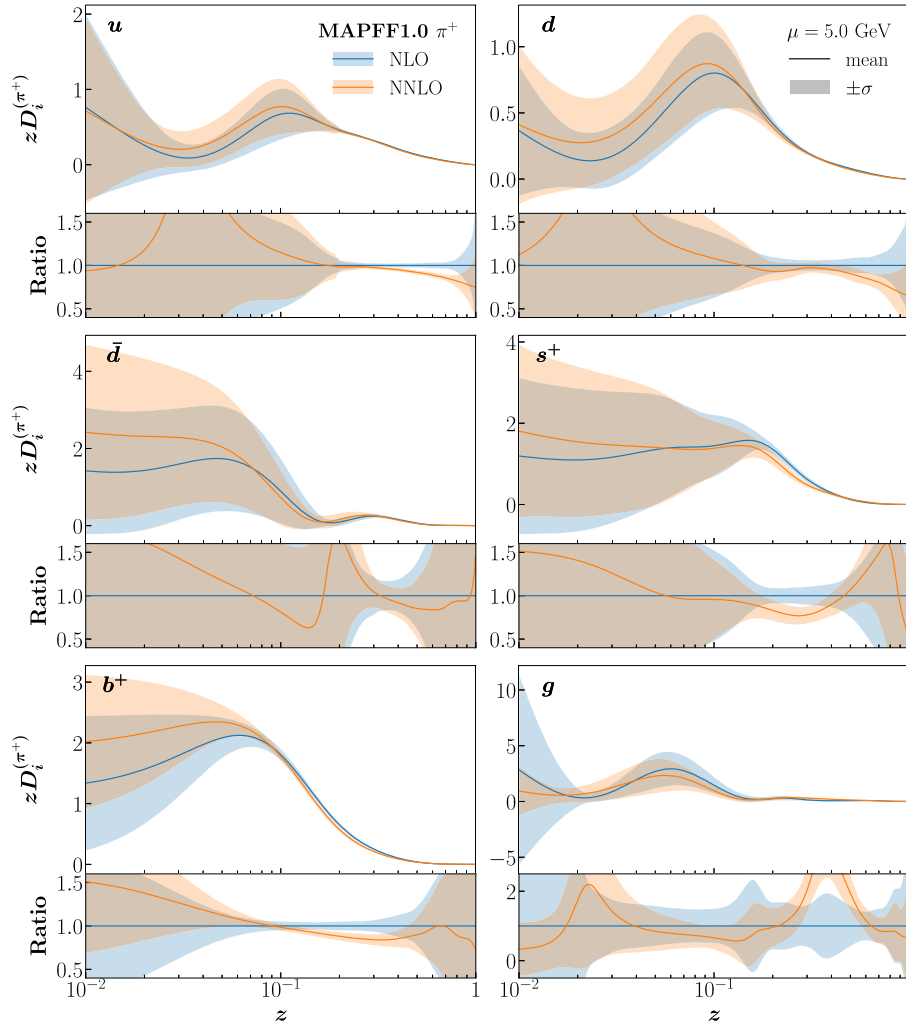
Fig. 1. Comparison of the NLO and NNLO FFs for positively charged pions. We display the $D_u^{\pi^+}$, $D_d^{\pi^+}$, $D_{\bar{d}}^{\pi^+}$, $D_{s^+}^{\pi^+}$, $D_{b^+}^{\pi^+}$ and $D_g^{\pi^+}$ FFs at $\mu = 5$ GeV. Expectation values and uncertainties correspond to the mean and standard deviation computed over the ensemble of FF replicas. For each FF we plot the absolute distributions in the upper panels and their ratio to the central value of the NLO FFs in the lower ones.

related, and is added in quadrature to the statistical uncertainty. This correlation model was singled out in the papers in which the COMPASS measurements were presented [25,37]. As already mentioned, the effect of this change is a significant reduction of the χ^2 per data point in comparison to the NLO pion fit of Ref. [1]; FFs are affected by fluctuations not large than a standard deviation, as one can infer by comparing Fig. 1 with Fig. 6 in Ref. [1], and as we have explicitly checked.

That being said, we repeated our NLO and NNLO fits for the pion FFs with two alternative decorrelation models: one in which the systematic uncertainties of the COMPASS data are 100% correlated; and one in which the systematic uncertainties in the COMPASS data are 100% uncorrelated. The fits are repeated for each value of Q_{cut} considered above. Our aim is to investigate whether the NLO and NNLO values of the global χ^2 per data point follow the same pattern observed in our default fits as Q_{cut} is varied.

The results are displayed in the left panel of Fig. 3, from which we draw two observations. First, the fit quality of the NNLO fit always remains worse than that of the NLO fit, irrespective of the correlation model used in the COMPASS data and of the value of Q_{cut}. Second, the correlation model affects the fit quality significantly: as the amount of correlation increases, not only the value of the global χ^2 per data point becomes higher, but also the deterioration of the fit quality occurs at larger values of Q_{cut}. Furthermore, we have explicitly checked the effect of the decorrelation

model on the fitted FFs. We have generally found that, irrespective of the value of Q_{cut} and of the perturbative order, pion FFs vary very little in comparison to our default if the systematic uncertainties in the COMPASS measurements are treated as fully uncorrelated. In particular, the variation is significantly smaller than that due to NNLO corrections, see Fig. 1. Note however that differences in the χ^2 per data point may be similar. For instance, with $Q_{\text{cut}} = 2$ GeV, the difference in χ^2 per data point between the default NLO and NNLO fits is 0.08; the same difference between the NNLO fits, in which the COMPASS systematic uncertainties are either partly correlated (our default) or fully uncorrelated, is 0.09. Distortions appear if the same systematic uncertainties are treated as fully correlated. However, the size of the distortion between fits with the same value of Q_{cut} typically does not exceed one standard deviation. These results illustrate the paramount importance of a careful estimate of experimental correlations – and of their proper treatment in the fit – to correctly interpret the fit quality in terms of χ^2 per data point.

4. Summary and outlook

In this paper we have extended the determination of NLO pion FFs of Ref. [1] in two respects. First, pion SIA and SIDIS measurements have now been analysed up to NNLO accuracy in perturbative QCD. Second, we have also determined companion kaon FF
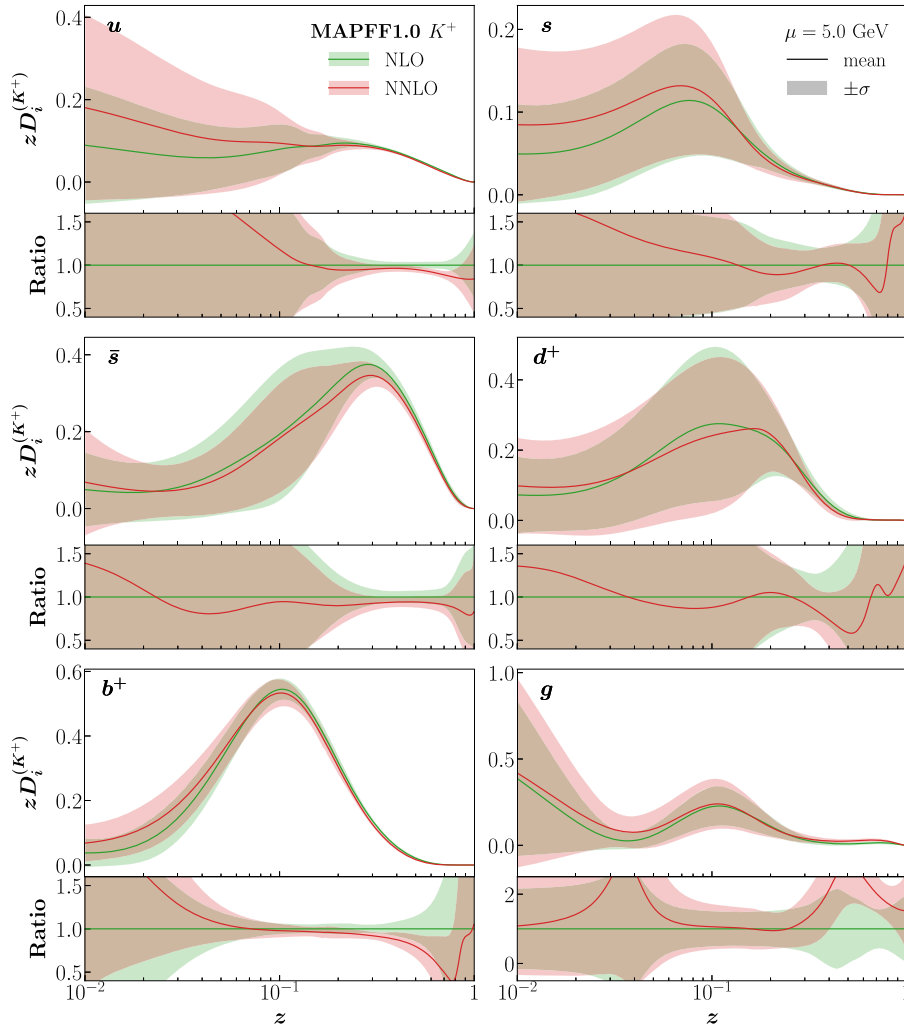
Fig. 2. Same as Fig. 1 for kaons, now displaying $D_u^{K^+}$, $D_s^{K^+}$, $D_{\bar{s}}^{K^+}$, $D_{d^+}^{K^+}$, $D_{b^+}^{K^+}$ and $D_g^{K^+}$.
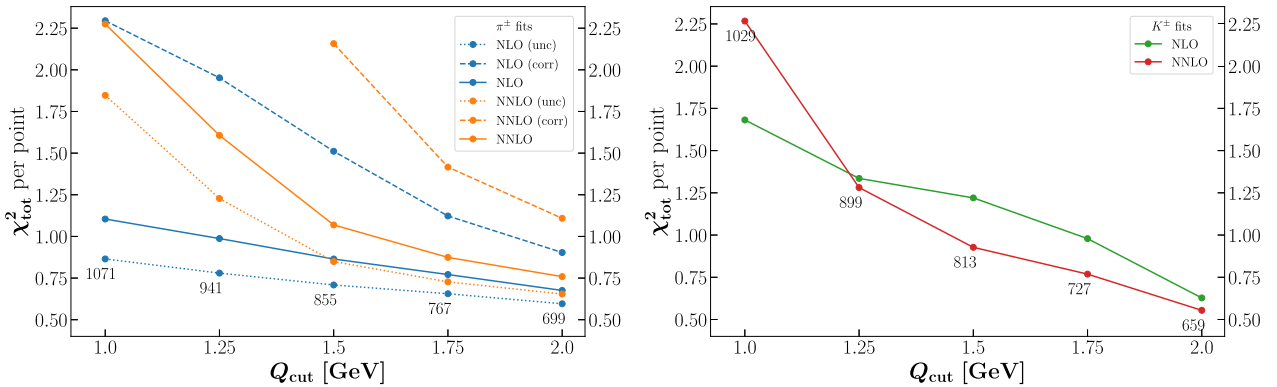

Fig. 3. The value of the total χ^2 per data point as a function of the cut on Q, Q_{cut}, applied to the SIDIS data in the pion (left) and kaon (right) FF fits. For each value of Q_{cut}, the number of data points included in the fits are also displayed. Both NLO and NNLO fits are considered. In the case of the fit of pion FFs, various correlation models for the COMPASS data are taken into account, see the text for details.

sets. Our study is based on a consolidated framework that combines a neural-network parametrisation of FFs with a Monte Carlo representation of their uncertainties. This framework ensures that model bias is reduced as much as possible, and that experimental and PDF uncertainties are faithfully propagated into FFs.

We have found that inclusion of NNLO corrections does not improve the quality of the pion FF fit, as measured by the χ^2 per data point, but it does for the kaon FF fit. Although the modifica-

tions of the NNLO FFs are qualitatively as expected with respect to the NLO FFs, the reason for the quantitative behaviour requires further investigations, possibly in the context of a benchmark with other FF sets, such as those determined in Ref. [22]. As also noted in Ref. [22], poorly known power corrections, beyond the leading-twist factorisation formalism used here, may play a role in the kinematic region covered by current SIDIS measurements. Indeed, we have observed a fast deterioration of the fit quality if the cut

on the virtuality of the SIDIS process is lowered, with the deterioration in the NNLO fit being more remarkable than in the NLO fit. We have finally exposed the importance of a correct estimation and treatment of experimental correlations to interpret the fit quality in terms of the χ^2 per data point.

Our NNLO pion and kaon FF sets, being the only ones to be publicly delivered to date, could be used in a number of computations that require a matching perturbative accuracy. For example, to make predictions of SIDIS cross sections measured by the future EIC at higher energy. Or to determine, for the first time at NNLO, longitudinally polarised PDFs from a simultaneous analysis of polarised inclusive deep-inelastic scattering and SIDIS measurements. Or else to serve as baseline for the parametrisation of transverse-momentum-dependent FFs.

The results presented in this paper have been obtained with the public code available in Ref. [24], see

https://github.com/MapCollaboration/MontBlanc.

For each perturbative order and hadron species (pion and kaon), we deliver the FF sets for the positively charged hadrons, for the negatively charged hadrons and for their sum. The names of the FF sets are as follows:

- NLO, pion: `MAPFF10NLOPIp`, `MAPFF10NLOPIm`, `MAPFF10NLOPIsum`;
- NNLO, pion: `MAPFF10NNLOPIp`, `MAPFF10NNLOPIm`, `MAPFF10NNLOPIsum`;
- NLO, kaon: `MAPFF10NLOKAp`, `MAPFF10NLOKAm`, `MAPFF10NLOKAsum`;
- NNLO, kaon: `MAPFF10NNLOKAp`, `MAPFF10NNLOKAm`, `MAPFF10NNLOKAsum`.

These FF sets are available from Ref. [24], where notebooks containing reports of the fits are also provided, and from the LHAPDF library [23]. Note that the NLO pion FF sets replace those delivered in the previous paper [1].

Declaration of competing interest

The authors declare that they have no known competing financial interests or personal relationships that could have appeared to influence the work reported in this paper.

Data availability

Data are publicly available from https://github.com/MapCollaboration

Acknowledgements

References

[1] R.A. Khalek, V. Bertone, E.R. Nocera, Determination of unpolarized pion fragmentation functions using semi-inclusive deep-inelastic-scattering data, Phys. Rev. D 104 (3) (2021) 034007, arXiv:2105.08725.

[2] A. Metz, A. Vossen, Parton fragmentation functions, Prog. Part. Nucl. Phys. 91 (2016) 136–202, arXiv:1607.02521.

[3] NNPDF Collaboration, E.R. Nocera, R.D. Ball, S. Forte, G. Ridolfi, J. Rojo, A first unbiased global determination of polarized PDFs and their uncertainties, Nucl. Phys. B 887 (2014) 276–308, arXiv:1406.5539.

[4] NNPDF Collaboration, R.D. Ball, et al., Parton distributions for the LHC Run II, J. High Energy Phys. 04 (2015) 040, arXiv:1410.8849.

[5] NNPDF Collaboration, R.D. Ball, et al., Parton distributions from high-precision collider data, Eur. Phys. J. C 77 (10) (2017) 663, arXiv:1706.00428.

[6] R.D. Ball, et al., The path to proton structure at one-percent accuracy, arXiv:2109.02653.

[7] NNPDF Collaboration, R. Abdul Khalek, J.J. Ethier, J. Rojo, Nuclear parton distributions from lepton-nucleus scattering and the impact of an electron-ion collider, Eur. Phys. J. C 79 (6) (2019) 471, arXiv:1904.00018.

[8] R. Abdul Khalek, J.J. Ethier, J. Rojo, G. van Weelden, nNNPDF2.0: quark flavor separation in nuclei from LHC data, J. High Energy Phys. 09 (2020) 183, arXiv:2006.14629.

[9] R.A. Khalek, R. Gauld, T. Giani, E.R. Nocera, T.R. Rabemananjara, J. Rojo, nNNPDF3.0: evidence for a modified partonic structure in heavy nuclei, arXiv:2201.12363.

[10] R. Abdul Khalek, et al., Science requirements and detector concepts for the electron-ion collider: EIC yellow report, arXiv:2103.05419.

[11] J.C. Collins, D.E. Soper, G.F. Sterman, Factorization of hard processes in QCD, Adv. Ser. Dir. High Energy Phys. 5 (1989) 1–91, arXiv:hep-ph/0409313.

[12] M. Abele, D. de Florian, W. Vogelsang, Approximate NNLO QCD corrections to semi-inclusive DIS, Phys. Rev. D 104 (9) (2021) 094046, arXiv:2109.00847.

[13] M. Abele, D. de Florian, W. Vogelsang, Threshold resummation at N^3LL accuracy and approximate N^3LO corrections to semi-inclusive DIS, arXiv:2203.07928.

[14] P.J. Rijken, W.L. van Neerven, O (alpha-s**2) contributions to the longitudinal fragmentation function in e+ e- annihilation, Phys. Lett. B 386 (1996) 422–428, arXiv:hep-ph/9604436.

[15] P.J. Rijken, W.L. van Neerven, O (alpha-s**2) contributions to the asymmetric fragmentation function in e+ e- annihilation, Phys. Lett. B 392 (1997) 207–215, arXiv:hep-ph/9609379.

[16] P.J. Rijken, W.L. van Neerven, Higher order QCD corrections to the transverse and longitudinal fragmentation functions in electron - positron annihilation, Nucl. Phys. B 487 (1997) 233–282, arXiv:hep-ph/9609377.

[17] A. Mitov, S. Moch, A. Vogt, Next-to-next-to-leading order evolution of non-singlet fragmentation functions, Phys. Lett. B 638 (2006) 61–67, arXiv:hep-ph/0604053.

[18] S. Moch, A. Vogt, On third-order timelike splitting functions and top-mediated Higgs decay into hadrons, Phys. Lett. B 659 (2008) 290–296, arXiv:0709.3899.

[19] A.A. Almasy, S. Moch, A. Vogt, On the next-to-next-to-leading order evolution of flavour-singlet fragmentation functions, Nucl. Phys. B 854 (2012) 133–152, arXiv:1107.2263.

[20] D.P. Anderle, T. Kaufmann, M. Stratmann, F. Ringer, Fragmentation functions beyond fixed order accuracy, Phys. Rev. D 95 (5) (2017) 054003, arXiv:1611.03371.

[21] NNPDF Collaboration, V. Bertone, S. Carrazza, N.P. Hartland, E.R. Nocera, J. Rojo, A determination of the fragmentation functions of pions, kaons, and protons with faithful uncertainties, Eur. Phys. J. C 77 (8) (2017) 516, arXiv:1706.07049.

[22] I. Borsa, D. de Florian, R. Sassot, M. Stratmann, W. Vogelsang, Towards a global QCD analysis of fragmentation functions at next-to-next-to-leading order accuracy, arXiv:2202.05060.

[23] A. Buckley, J. Ferrando, S. Lloyd, K. Nordström, B. Page, M. Rüfenacht, M. Schönherr, G. Watt, LHAPDF6: parton density access in the LHC precision era, Eur. Phys. J. C 75 (2015) 132, arXiv:1412.7420.

[24] R.A. Khalek, V. Bertone, A. Khoudli, E.R. Nocera, Mapcollaboration/montblanc: Refuge du goûter, Feb. 2022.

[25] COMPASS Collaboration, C. Adolph, et al., Multiplicities of charged pions and charged hadrons from deep-inelastic scattering of muons off an isoscalar target, Phys. Lett. B 764 (2017) 1–10, arXiv:1604.02695.

[26] ALEPH Collaboration, D. Buskulic, et al., Inclusive pi+-, K+- and (p, anti-p) differential cross-sections at the Z resonance, Z. Phys. C 66 (1995) 355–366.

[27] DELPHI Collaboration, P. Abreu, et al., pi+-, K+-, p and anti-p production in Z0 —> q anti-q, Z0 —> b anti-b, Z0 —> u anti-u, d anti-d, s anti-s, Eur. Phys. J. C 5 (1998) 585–620.

[28] OPAL Collaboration, R. Akers, et al., Measurement of the production rates of charged hadrons in e+ e- annihilation at the Z0, Z. Phys. C 63 (1994) 181–196.

[29] TASSO Collaboration, R. Brandelik, et al., Charged pion, kaon, proton and anti-proton production in high-energy e+ e- annihilation, Phys. Lett. B 94 (1980) 444–449.

[30] TASSO Collaboration, M. Althoff, et al., Charged hadron composition of the final state in e^+e^- annihilation at high-energies, Z. Phys. C 17 (1983) 5–15.

[31] TASSO Collaboration, W. Braunschweig, et al., Pion, kaon and proton cross-sections in e^+e^- annihilation at 34-GeV and 44-GeV center-of-mass energy, Z. Phys. C 42 (1989) 189.

[32] Belle Collaboration, M. Leitgab, et al., Precision measurement of charged pion and kaon differential cross sections in e+e- annihilation at s=10.52 GeV, Phys. Rev. Lett. 111 (2013) 062002, arXiv:1301.6183.

[33] TOPAZ Collaboration, R. Itoh, et al., Measurement of inclusive particle spectra and test of MLLA prediction in e^+e^- annihilation at s**(1/2) = 58-GeV, Phys. Lett. B 345 (1995) 335–342, arXiv:hep-ex/9412015.

[34] BaBar Collaboration, J.P. Lees, et al., Production of charged pions, kaons, and protons in e^+e^- annihilations into hadrons at $\sqrt{s} = 10.54$ GeV, Phys. Rev. D 88 (2013) 032011, arXiv:1306.2895.

[35] TPC/Two Gamma Collaboration, H. Aihara, et al., Charged hadron inclusive cross-sections and fractions in e^+e^- annihiliation $\sqrt{s} = 29$ GeV, Phys. Rev. Lett. 61 (1988) 1263.

[36] SLD Collaboration, K. Abe, et al., Production of π^+, π^-, K^+, K^-, p and $\bar{p}$ in light (uds), c and b jets from Z^0 decays, Phys. Rev. D 69 (2004) 072003, arXiv:hep-ex/0310017.

[37] COMPASS Collaboration, C. Adolph, et al., Multiplicities of charged kaons from deep-inelastic muon scattering off an isoscalar target, Phys. Lett. B 767 (2017) 133–141, arXiv:1608.06760.

[38] HERMES Collaboration, A. Airapetian, et al., Multiplicities of charged pions and kaons from semi-inclusive deep-inelastic scattering by the proton and the deuteron, Phys. Rev. D 87 (2013) 074029, arXiv:1212.5407.

[39] Belle Collaboration, R. Seidl, et al., Update of inclusive cross sections of single and pairs of identified light charged hadrons, Phys. Rev. D 101 (9) (2020) 092004, arXiv:2001.10194.

[40] D. de Florian, M. Epele, R.J. Hernandez-Pinto, R. Sassot, M. Stratmann, Parton-to-kaon fragmentation revisited, Phys. Rev. D 95 (9) (2017) 094019, arXiv:1702.06353.

[41] Jefferson Lab Angular Momentum (JAM) Collaboration, E. Moffat, W. Melnitchouk, T.C. Rogers, N. Sato, Simultaneous Monte Carlo analysis of parton densities and fragmentation functions, Phys. Rev. D 104 (1) (2021) 016015, arXiv:2101.04664.

[42] D. de Florian, R. Sassot, M. Epele, R.J. Hernández-Pinto, M. Stratmann, Parton-to-pion fragmentation reloaded, Phys. Rev. D 91 (1) (2015) 014035, arXiv:1410.6027.

[43] N. Sato, J.J. Ethier, W. Melnitchouk, M. Hirai, S. Kumano, A. Accardi, First Monte Carlo analysis of fragmentation functions from single-inclusive e^+e^- annihilation, Phys. Rev. D 94 (11) (2016) 114004, arXiv:1609.00899.

[44] V. Bertone, S. Carrazza, E.R. Nocera, Reference results for time-like evolution up to $\mathcal{O}(\alpha_s^3)$, J. High Energy Phys. 03 (2015) 046, arXiv:1501.00494.

[45] V. Bertone, S. Carrazza, J. Rojo, APFEL: a PDF evolution library with QED corrections, Comput. Phys. Commun. 185 (2014) 1647–1668, arXiv:1310.1394.

[46] V. Bertone, APFEL++: a new PDF evolution library in C++, PoS DIS2017 (2018) 201, arXiv:1708.00911.

[47] M. Cacciari, P. Nason, C. Oleari, Crossing heavy-flavor thresholds in fragmentation functions, J. High Energy Phys. 10 (2005) 034, arXiv:hep-ph/0504192.

[48] S. Agarwal, K. Mierle, Others, Ceres solver, http://ceres-solver.org.

[49] R. Abdul Khalek, V. Bertone, On the derivatives of feed-forward neural networks, arXiv:2005.07039.

[50] D.P. Anderle, F. Ringer, M. Stratmann, Fragmentation functions at next-to-next-to-leading order accuracy, Phys. Rev. D 92 (11) (2015) 114017, arXiv:1510.05845.

[51] A. Accardi, D.P. Anderle, F. Ringer, Interplay of threshold resummation and hadron mass corrections in deep inelastic processes, Phys. Rev. D 91 (3) (2015) 034008, arXiv:1411.3649.

[52] J.V. Guerrero, J.J. Ethier, A. Accardi, S.W. Casper, W. Melnitchouk, Hadron mass corrections in semi-inclusive deep-inelastic scattering, J. High Energy Phys. 09 (2015) 169, arXiv:1505.02739.

[53] M. Boglione, J. Collins, L. Gamberg, J.O. Gonzalez-Hernandez, T.C. Rogers, N. Sato, Kinematics of current region fragmentation in semi-inclusive deeply inelastic scattering, Phys. Lett. B 766 (2017) 245–253, arXiv:1611.10329.

[54] M. Boglione, A. Dotson, L. Gamberg, S. Gordon, J.O. Gonzalez-Hernandez, A. Prokudin, T.C. Rogers, N. Sato, Mapping the kinematical regimes of semi-inclusive deep inelastic scattering, J. High Energy Phys. 10 (2019) 122, arXiv:1904.12882.

[55] M. Boglione, M. Diefenthaler, S. Dolan, L. Gamberg, W. Melnitchouk, D. Pitonyak, A. Prokudin, N. Sato, Z. Scalyer, New tool for kinematic regime estimation in semi-inclusive deep-inelastic scattering, arXiv:2201.12197.